correlates with the emergence of a soft spin-flip ($\delta S_z = 1$) mode of vanishingly low energy close to $\omega_{SDE} - E_Z$.

The inelastic LS results also enable the construction of a spin-configuration phase diagram at filling factors $\nu = 6$ and $\nu = 2$. Figure 5 shows the diagram obtained from data measured in four DQW samples that differ in density and Δ_{SAS}. The diagram confirms that at large B_T and relatively small Δ_{SAS}, the bilayers are in the spin-polarized phase P. At smaller magnetic fields such that $\Delta_{SAS} \gg E_Z$, the bilayers are in the spin-unpolarized phase U. The new phase D occurs at intermediate Δ_{SAS} and E_Z, when the $q \approx 0$ tunneling spin-excitation becomes soft. The phase diagram in Fig. 5 is consistent with the predictions of (*17*). The soft-mode having $\delta S_z = +1$ suggests an order-parameter associated with the operator $\delta S^+ = \delta(S_x - iS_y)$. Such broken-symmetry is consistent with a canted AF phase, as proposed in (*16, 17*).

The LS spectra of phase D have an intriguing T dependence in which SDE excitations at $\nu = 2$ reappear for $T \geq 0.5$ K (*15*). This unexpected behavior is evidence of a reversal $D \rightarrow U$ transformation at a temperature $T_c \cong 0.5$ K. We have studied this effect as a function of tilt angle. Figure 2C shows T_c measured at 30° (solid circles). Comparison with the 0° results (dashed line) reveals an enhanced stability of phase D at finite tilt. From LS spectra obtained at $\nu \simeq 6$ we determined that changing the tilt angle from 0° to 30° reduces Δ_{SAS} by about 0.05 meV, as predicted by current theory (*22*). Thus, the results in Fig. 2B indicate that the increased stability of phase D correlates with a reduction in Δ_{SAS}. This behavior is consistent with the proposal that phase D is a Kosterlitz-Thouless state with a transition temperature T_c (*17*).

Finally, measurements of SW modes yield precise determinations of E_Z over a wide range of B_T. To this effect, we carried out a fit by means of the expression $E_Z = (g_o - cB/2)\mu_B B$, which incorporates a small quadratic correction to the g factor (*23*). The best fit is shown as dotted lines in Figs. 3 and 4. These determinations enable the evaluation of the Zeeman energy at field close to $\nu = 2$. We find in Fig. 4 that the energy of the SDE tunneling mode reaches the value $\omega_{SDE} = E_Z$ when the SDE peak disappears with the emergence of phase D. This result is a strong indication that the $U \rightarrow D$ transition might be continuous. Experiments carried out at lower temperatures could offer further insights. The instability could also be investigated by activated magnetotransport (*24*).

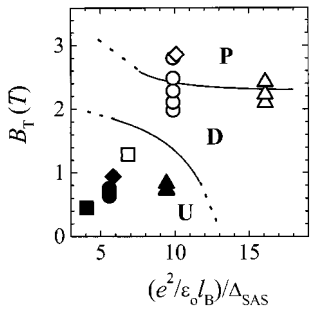

Fig. 5. Phase diagram of electron bilayers at even values of ν and $T = 0.2$ K. The total magnetic field B_T is plotted here against the reciprocal tunneling gap in units of the Coulomb interaction energy ($e^2/\epsilon_o l_B$), where ϵ_o is the dielectric constant. Solid lines indicate the positions of the phase boundaries determined from experiment. Dotted lines are introduced to give continuity to the boundaries. The samples are GaAs quantum wells of different densities. Squares, $n = 6.2 \times 10^{10}$ cm^{-2}; circles, $n = 9.9 \times 10^{10}$ cm^{-2}; triangles, $n = 1.05 \times 10^{11}$ cm^{-2}; and diamonds, $n = 1.44 \times 10^{11}$ cm^{-2}. Open symbols are for $\nu = 2$ and closed symbols for $\nu = 6$.

References and Notes

1. R. E. Prange and S. M. Girvin, Eds., *The Quantum Hall Effect* (Springer, New York, ed. 2, 1990).
2. T. Chakraborty and P. Pietilainen, *The Quantum Hall Effects: Integral and Fractional*, vol. 85 of the Springer Series in Solid State Sciences (Springer, New York, ed. 2, 1995).
3. S. Das Sarma and A. Pinczuk, Eds., *Perspectives in Quantum Hall Effects* (Wiley, New York, 1996).
4. K. Moon *et al.*, *Phys. Rev. B* **51**, 5138 (1995).
5. J. P. Eisenstein, in (*3*), pp. 37–70.
6. M. Shayegan, *ibid.*, pp. 343–384.
7. S. L. Sondhi *et al.*, *Rev. Mod. Phys.* **69**, 315 (1997).
8. S. M. Girvin, A. H. MacDonald, P. M. Platzman, *Phys. Rev. B* **33**, 2481 (1985).
9. H. A. Fertig, *ibid.* **40**, 1087 (1989).
10. A. H. MacDonald, P. M. Platzman, G. S. Boebinger, *Phys. Rev. Lett.* **65**, 775 (1990).
11. L. Brey, *ibid.*, p. 903.
12. R. K. Kamilla and J. K. Jain, *Phys. Rev. B* **55**, R13417 (1997).
13. C. Kallin and B. I. Halperin, *ibid.* **30**, 5655 (1984).
14. A. Pinczuk *et al.*, *Bull. Am. Phys. Soc.* **41**, 482 (1996); A. S. Plaut, *ibid.*, p. 590.
15. V. Pellegrini *et al.*, *Phys. Rev. Lett.* **78**, 310 (1997).
16. L. Zheng *et al.*, *ibid.*, p. 2453.
17. S. Das Sarma *et al.*, *ibid.* **79**, 917 (1997).
18. G. F. Giuliani and J. J. Quinn, *Phys. Rev. B* **31**, 6228 (1985).
19. G. S. Boebinger, H. W. Jiang, L. N. Pfeiffer, K. W. West, *Phys. Rev. Lett.* **64**, 1793 (1990).
20. A. S. Plaut *et al.*, *Phys. Rev. B* **55**, 9282 (1997).
21. Y. Yafet, *Phys. Rev.* **152**, 858 (1966). For the same reason, the tilted field geometry allows inelastic light scattering from spin-flip intersubband modes with $\delta S_z = \pm 1$. We have found, however, little evidence of such modes in the resonant inelastic light scattering spectra at ν close to 2. This may stem from the presence of several relaxation channels for the intersubband spin-flip modes and the consequent broadening of the peak.
22. J. Hu and A. H. MacDonald, *Phys. Rev. B* **46**, 12554 (1992).
23. M. Dobers, K. v. Klitzing, G. Weiman, *ibid.* **38**, 5453 (1988); M. J. Snelling *et al.*, *ibid.* **44**, 11345 (1991).
24. A. Sawada *et al.*, *Phys. Rev. Lett.* **80**, 4534 (1998).

25. We thank K. W. Baldwin for magnetotransport measurements.

7 April 1998; accepted 23 June 1998

Preparation of Photonic Crystals Made of Air Spheres in Titania

Judith E. G. J. Wijnhoven and Willem L. Vos*

Three-dimensional crystals of air spheres in titania (TiO_2) with radii between 120 and 1000 nanometers were made by filling the voids in artificial opals by precipitation from a liquid-phase chemical reaction and subsequently removing the original opal material by calcination. These macroporous materials are a new class of photonic band gap crystals for the optical spectrum. Scanning electron microscopy, Raman spectroscopy, and optical microscopy confirm the quality of the samples, and optical reflectivity demonstrates that the crystals are strongly photonic and near that needed to exhibit band gap behavior.

There is currently an intensive effort to develop porous materials with a wide range of pore sizes up to 30 nm that open up new opportunities in catalysis and separation technology (*1, 2*). These materials are made by using self-organizing systems, such as surfactant liquids and biological systems as templates for the deposition of inorganic materials. An emerging field that benefits from crystalline macroporous materials (*3*) is the field of photonic crystals, that is, three-dimensional (3D) dielectric composites with lattice spacings of the order of wavelengths of light (about 500 nm) (*4*). These crystals can be used to create photonic band gaps (frequency ranges that will not propagate light because of multiple Bragg reflections) (*5*) that induce useful optical properties, such as inhibition of spontaneous emission or photon localization (*4*). To achieve band gaps for the visible and infrared spectrum, several challenges exist: both constituent materials of the crystal should be topologically interconnected (*6*) and the ratio of their refractive indices n should at least be 2 (*5*). We have synthesized crystals of air spheres in titania that meet these criteria. In

Van der Waals-Zeeman Instituut, Universiteit van Amsterdam, Valckenierstraat 65, NL-1018 XE Amsterdam, Netherlands. http://www.wins.uva.nl/research/scm

*To whom correspondence should be addressed. E-mail: wvos@phys.uva.nl

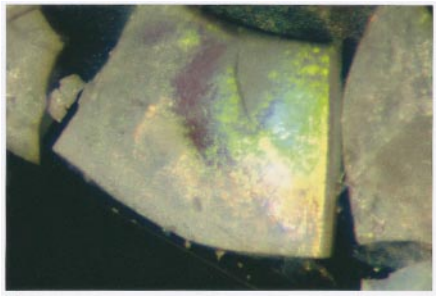

Fig. 1. Photograph of crystals of air spheres in TiO_2. The crystals were made from templates consisting of particles with radii of 225 nm. The width of the field of view is 0.5 mm. The bright blue and green reflections are optical Bragg reflections from the crystals. Several colors appear because the angle of incidence of the illuminating white beam varies with respect to the crystal planes.

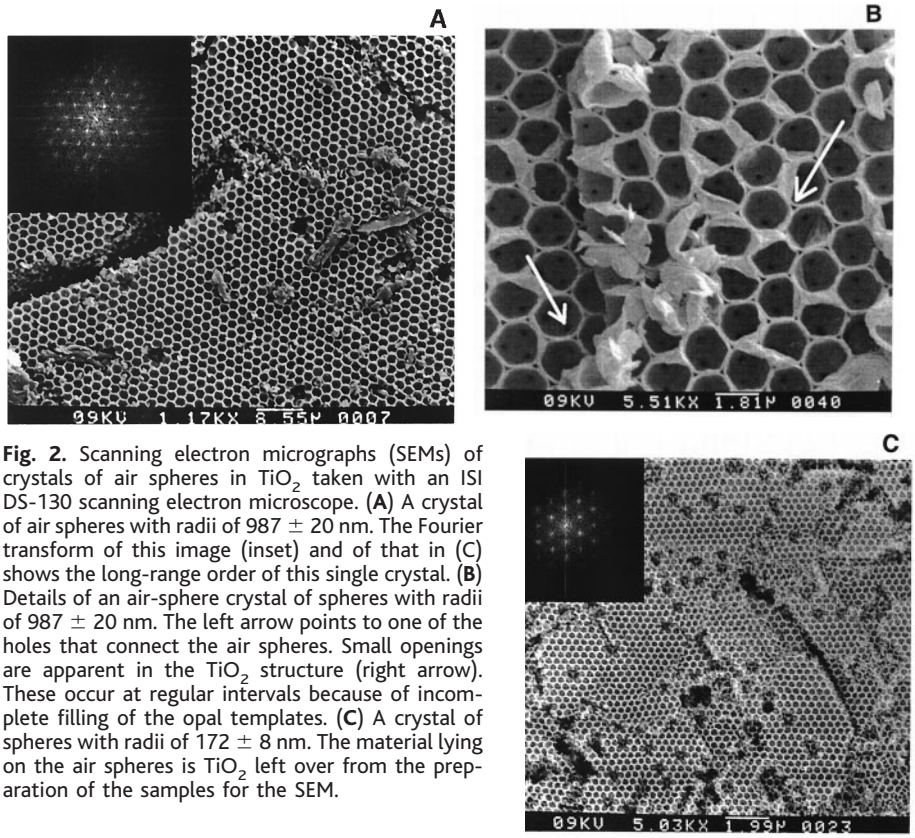

Fig. 2. Scanning electron micrographs (SEMs) of crystals of air spheres in TiO_2 taken with an ISI DS-130 scanning electron microscope. (**A**) A crystal of air spheres with radii of 987 ± 20 nm. The Fourier transform of this image (inset) and of that in (C) shows the long-range order of this single crystal. (**B**) Details of an air-sphere crystal of spheres with radii of 987 ± 20 nm. The left arrow points to one of the holes that connect the air spheres. Small openings are apparent in the TiO_2 structure (right arrow). These occur at regular intervals because of incomplete filling of the opal templates. (**C**) A crystal of spheres with radii of 172 ± 8 nm. The material lying on the air spheres is TiO_2 left over from the preparation of the samples for the SEM.

addition to their use as photonic crystals, such macroporous crystals might have applications as collectors of solar energy (*7*), devices for quantum confinement (*8*), and refractive lenses for the microfocusing of x-rays or neutrons (*9*).

Two approaches have been used to create photonic crystals: engineering by microlithography (*10*) and colloidal suspensions that spontaneously form colloidal crystals or artificial opals (*11, 12*). With microengineering methods, it has not yet been feasible to produce true 3D crystals, and for colloids and opals, it has been difficult to achieve high *n* ratios and obtain the desired interconnectedness. The latter feature is readily achieved, however, in template-grown porous materials (*1, 2*), but the question remains whether structures with crystalline order can be fabricated. Indeed, Velev *et al.* have made 3D crystalline arrays of macropores in silica that were replicated from colloidal crystals (*13*). Another challenge is to make pores in materials with sufficiently high *n*. Interestingly, Imhof and Pine (*14*) have used surfactants to pattern macropores in titania (TiO_2), which has a much higher *n* than silica (>2.5 compared with 1.45). Here we used opals to fabricate crystals of air spheres in a material with a high *n*, yielding photonic crystals with a high refractive index ratio (Figs. 1 and 2). These porous crystals were prepared as follows. First, the template was assembled from a self-organizing system, and second, the desired solid material was brought into the voids of the template by precipitation from a chemical reaction. In the last step, the macroporous sample was obtained by removing the original template material by calcination.

The template we used was a 3D colloidal crystal dried to form an artificial opal. The final radius of the air spheres and the thickness of the TiO_2 walls were controlled by the radius of the original colloidal spheres. Monodisperse polystyrene (PS) latex spheres (*15*) with radii between 180 and 1460 nm were used as received from the supplier (Duke Scientific). The colloidal suspensions were loaded in long, flat glass capillaries of 0.3-mm thickness and 3-mm width, and dense colloidal crystals were grown by sedimentation of the spheres at accelerations of ~400*g*. The samples were centrifuged for 2 to 48 hours to obtain polycrystalline sediments >10 mm in length. We verified by small-angle x-ray diffraction that such crystals had a face-centered cubic (fcc) structure (*16, 17*). Theoretical calculations by Sözüer *et al.* (*18*) showed that fcc crystals of air spheres have photonic band gaps. In addition, the colloidal particles were strongly localized about their lattice sites; hence, the opals were well ordered (*17*). The opal was obtained from the colloidal crystals by evaporating the suspending liquid from the capillary. Slow evaporation is necessary to minimize the number of cracks that appear in the opal, which can form because the particle density in the resulting opal is greater than that in the original colloidal crystal (~74 volume % versus ~50 volume %).

In the second step of the process, the voids in the opals were filled with the desired material by precipitation from a liquid-phase chemical reaction. The precursor liquid penetrates the voids in the opal by capillary forces, which takes about 10 min to 1 hour. To obtain TiO_2, we used as a precursor a solution of tetrapropoxy-titane (TPT) in ethanol, in proportions ranging from 20 to 100 volume %. The precursor was handled inside a nitrogen-purged glove box because of its high reactivity to water. The samples were taken out of the box to let the TPT react with water from the atmosphere. We repeated the cycle of penetration, reaction, and drying up to eight times (depending on the concentration of TPT) to ensure that the voids in the opal were sufficiently filled. After an opal is filled with solid material, the particles appear jagged in scanning electron micrographs (SEMs) (not shown here) because they are covered with a shell of this solid. As an alternative to chemical precipitation, we also explored precipitation of crystals from a saturated solution, using aqueous sodium chloride solutions as precursors. This resulted in crystals of air spheres in sodium chloride.

In the third step of the process PS particles were removed. Calcination is the common method in the preparation of inorganic porous materials made with organic templates (*2*). Therefore, we slowly heated the samples (5°C per minute) to 450°C, and the PS latex was gasified and burned. The SEMs of the resulting macroporous structures (Fig. 2) show an ordered hexagonal pattern of spherical holes in the TiO_2 structure. Sharp peaks in the Fourier transform of these images (insets in Fig. 2, A and C) confirm the presence of long-range crystalline order. The next lower layer of air spheres is visible in the SEMs (Fig. 2B), as well as the holes that connect each air sphere to its nearest neighbors in the next layer. Both the TiO_2 structure and the air spheres are connected,

which is favorable to realize band gaps in photonic crystals (*6*). The SEMs show that the air-sphere samples have lattice parameters that are about 33% less than those of the original opals. Similar results have been observed in the preparation of other porous materials (*2*). Such large shrinkage almost completely compacts the solid network (*1, 2*) (the TiO_2 structure in our case); therefore, it is unlikely that the *n* of the TiO_2 structure itself is reduced by the presence of nanopores. A drawback of the shrinkage is that the opal sediment breaks into smaller pieces of typically 0.5-mm length. We attribute the occurrence of ruptures (seen in Fig. 2) to this shrinkage process. Nevertheless, the long-range order of the air-sphere crystal remains. As an alternative to calcination, we attempted to dissolve the PS latex particles in organic solvents. Although this process selectively removes PS, it yields a disordered air-sphere structure. The original crystalline order of the opal may be destroyed if the PS latex swells before it dissolves.

There are small openings in the middle of each of the triangular intersections of TiO_2 (Fig. 2B). These openings are likely caused by the thin channels between the voids in the opal filling up more rapidly than the voids themselves, blocking further diffusion of the precursor materials. These small extra openings decrease the volume fraction of TiO_2, but a high volume fraction is needed for strong photonic effects (*12*). Detailed calculations by Busch and John (*19*), however, reveal that such voids in fact enlarge photonic band gaps. Vacancies in the air-sphere structures are visible in Fig. 2. We surmise that these are caused by incomplete filling of the opals by the precursor, because the number of vacancies increased if a lower TPT concentration was used or if fewer filling cycles were used. Nevertheless, the vacancies do not disrupt the long-range order.

Optical Raman spectroscopy (Fig. 3) of the TiO_2 structure reveals five strong Raman bands at 143, 198, 400, 518, and 640 cm^{-1}. This is in agreement with data on anatase (*20*), the stable polymorph of TiO_2 below 700°C, but not with data on other TiO_2 polymorphs such as rutile (Fig. 3). We did not observe Raman active peaks of any impurities, such as other TiO compounds (Ti_2O_3), or other chemical reaction products. The anatase structure has an *n* that increases from 2.5 at a wavelength of 700 nm to 2.8 at 400 nm (*21*).

Visually, the air-sphere crystals show a beautiful iridescence in reflected light, similar to opals (Fig. 1). This allows us to select crystals before further optical experiments. A typical reflectivity spectrum (Fig. 4) of a polycrystalline sample reveals a broad peak centered at 14,900 cm^{-1} that is a Bragg reflection peak of the hexagonal air-sphere layers [the (111) reflection peak of the fcc air crystals]. In strongly photonic crystals, the lattice spacing and the average *n* of the crystal are related to the frequency of a Bragg reflection (*12*). From the lattice spacing determined from the SEMs, we derived an average *n* between 1.18 and 1.29 for the various air-sphere crystals. Using effective medium models for the average *n*, and taking into account the *n* of anatase (*21*), we calculated that the density of TiO_2 is between 12 and 20 volume %, with the higher densities occurring for the larger spheres. The full width at half maximum of a Bragg peak in reflection is directly related to the width of the stopband in the dispersion curves and can be considered as a measure of the coupling between light and photonic crystals, that is, the photonic strength (*22*). We found a relative width of about 13% for the width of the stopgap in the fcc (111) direction (L gap). For comparison, we plotted a Bragg reflection of a colloidal crystal of silica spheres. These data illustrate that the air-sphere crystals are much more strongly photonic than any colloidal crystal or opal (*11, 12*). From theoretical work, the transition to a full photonic band gap is expected for a stopgap width in the range of 15 to 20% (*4, 5*).

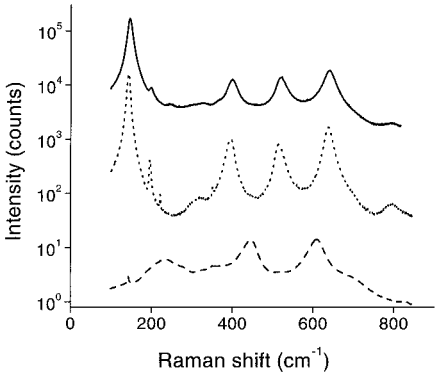

Fig. 3. Raman spectrum of a crystal of air spheres in TiO_2 (solid curve). The dotted curve is for anatase (Aldrich), shifted down by a factor of 10, and the dashed curve for rutile (Acros Organics), shifted down by a factor of 1000. The peaks of the air-sphere sample agree very well with the vibration frequencies of the Raman active phonons of the anatase structure of TiO_2 (*20*). The samples were excited with light of wavelengths 488 or 514 nm, and the scattered light was collected by a Dilor XY spectrometer, equipped with a liquid nitrogen–cooled charge-coupled device detector. From top to bottom, the spectra were collected for 30, 25, and 150 s.

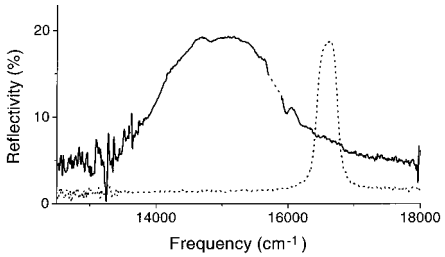

Fig. 4. Optical reflectance spectrum of crystals of air spheres in TiO_2. The crystals were made from templates consisting of particles with radii of 241 nm. The dashed curve is the reflectance spectrum of a dense colloidal crystal of silica spheres (radii of 101 nm) in water, with a density of 57 volume %. The incident beam emanated from a Xe white light source, and the reflected light was analyzed with a Bio-Rad FTS-60 Fourier transform spectrometer. The reflectance is not defined in a narrow band around 15,800 cm^{-1} because of interference by a reference laser beam inside the spectrometer.

References and Notes

1. C. T. Kresge *et al*., *Nature* **359**, 710 (1992); J. S. Beck *et al*., *J. Am. Chem. Soc.* **114**, 10834 (1992); D. Zhao *et al*., *Science* **279**, 548 (1998).
2. For reviews see, N. K. Raman, M. T. Anderson, C. J. Brinker, *Chem. Mater.* **8**, 1682 (1996); S. Mann and G. A. Ozin, *Nature* **382**, 313 (1996).
3. The International Union of Pure and Applied Chemistry (IUPAC) definition is that micropores are pores with radii $r < 1$ nm, mesopores have $1 < r < 25$ nm, and macropores have $r > 25$ nm.
4. E. Yablonovitch, *Phys. Rev. Lett.* **58**, 2059 (1987); S. John, *ibid*., p. 2486.
5. See, for example, *Development and Applications of Materials Exhibiting Photonic Band Gaps*, C. M. Bowden, J. P. Dowling, H. O. Everitt, Eds., *J. Opt. Soc. Am. B* **10**, 280 (1993); J. D. Joannopoulos, R. D. Meade, J. N. Winn, *Photonic Crystals* (Princeton Univ. Press, Princeton, NJ, 1995).
6. E. N. Economou and M. M. Sigalas, *Phys. Rev. B* **48**, 13434 (1993).
7. B. O'Regan and M. Grätzel, *Nature* **353**, 737 (1993).
8. L. C. Kimerling, K. D. Kolenbrander, J. Michel, J. Palm, in *Solid State Physics*, H. Ehrenreich and D. Turnbull, Eds. (Academic Press, Boston, 1997), pp. 333–381.
9. A. Snigirev, V. Kohn, I. Snigireva, B. Lengeler, *Nature* **384**, 49 (1996).
10. V. Arbet-Engels, E. Yablonovitch, C. C. Cheng, A. Scherer, in *Microcavities and Photonic Band Gaps*, C. Weisbuch and J. G. Rarity, Eds. (Kluwer, Dordrecht, Netherlands, 1996); T. F. Krauss, R. M. DeLaRue, S. Brand, *Nature* **383**, 699 (1996).
11. S. G. Romanov *et al*., *Phys. Status Solidi* **164**, 169 (1997); V. N. Bogomolov *et al*., *Phys. Rev. E* **55**, 7619 (1997), and references therein.
12. W. L. Vos, R. Sprik, A. van Blaaderen, A. Imhof, A. Lagendijk, G. H. Wegdam, *Phys. Rev. B* **53**, 16231 (1996); *ibid.* **55**, 1903(E) (1997); W. L. Vos, M. Megens, C. M. van Kats, P. Bösecke, *J. Phys. Condens. Matter* **8**, 9503 (1996).
13. O. D. Velev, T. A. Jede, R. F. Lobo, A. M. Lenhoff, *Nature* **389**, 447 (1997).
14. A. Imhof and D. J. Pine, *ibid*., p. 948.
15. M. Megens, C. M. van Kats, P. Bösecke, W. L. Vos, *Langmuir* **13**, 6120 (1997).
16. ———, *J. Appl. Cryst.* **30**, 637 (1997).
17. W. L. Vos, M. Megens, C. M. van Kats, P. Bösecke, *Langmuir* **13**, 6004 (1997).
18. H. S. Sözüer, J. W. Haus, R. Inguva, *Phys. Rev. B* **45**, 13962 (1992).
19. K. Busch and S. John, *Phys. Rev. E*, in press.
20. J. F. Mammone, S. K. Sharma, M. Nicol, *Solid State Commun.* **34**, 799 (1980).
21. J. Bartels *et al*., Ed., *Landolt-Börnstein, Zahlenwerte und funktionen, Optische Konstanten* (Springer-Verlag, Berlin, 1962), II Band, 8. Teil.
22. W. L. Vos, M. Megens, J. E. G. J. Wijnhoven, paper CFB6 presented at the Conference on Lasers and Electro Optics, Glasgow, 13 to 18 September 1998.

23. We thank M. Thijssen and W. Takkenberg for help with experiments; M. Megens, A. van Blaaderen, and S. John for discussions; and A. Lagendijk for encouragement and support. This work is part of the research program of the Stichting voor Fundamenteel Onderzoek der Materie, which is financially supported by the Nederlandse Organisatie voor Wetenschappelijk Onderzoek.

11 May 1998; accepted 1 July 1998